ADVANCES IN MULTI-MODAL CHARACTERIZATION OF STRUCTURAL MATERIALS

# Stress and Deformation Distribution and Microstructure Changes Around Pin-Loaded Holes in Medium Manganese Steel Plates

Y. DU [1,4] X.H. GAO,[1,5] Z.W. DU,[2] Y. DONG,[1] B. ZHANG,[1] R.D.K. MISRA,[3] H.Y. WU,[1] and L.X. DU[1,6]

1.—State key Laboratory of Rolling and Automation, Northeastern University, Shenyang 110819, Liaoning, China. 2.—National Engineering Laboratory for Hydrometallurgical Cleaner Production Technology, Institute of Process Engineering, Chinese Academy of Sciences, Beijing 100190, China. 3.—Laboratory for Excellent in Advanced Steel Research, Department of Metallurgical, Materials and Biomedical Engineering, University of Texas at EI Paso, EI Paso, TX 79968-0521, USA. 4.—e-mail: duyu_2016@foxmail.com. 5.—e-mail: gaoxh@ral.neu.edu.cn. 6.—e-mail: dulx@ral.neu.edu.cn

The effects of traction load, plate thickness, and pin radius on stress and deformation distribution were investigated by simulation symmetrical pin traction experiment and analytical calculation methods. At the beginning of traction, both contact angle and maximum stress increase with the traction load. As the traction continues, maximum stress is steady and only the contact angle increases with the traction load. The stress concentration increases with the decrease of pin radius and does not change with other parameters under the same pin radius. The increase of specimen thickness can only reduce the contact angle but does not lessen the stress concentration, and thicker specimens can bear more traction load when reaching the same contact angle. Strengthening during deformation is caused not only by the increase of dislocation density in martensite matrix but also by retained austenite (RA) strain-induced martensite transformation (SIMT), which is conducive to the transfer of plastic deformation.

## Abbreviations

$D$    Diameter of the hole
$\Delta D$    Diameter increase along the direction of the traction
$F$    Traction force
$h$    Thickness of the specimen
$\Delta h_0$    Maximum unilateral thickening of the specimen
$p$    Normal edge force
$p_0$    Force resultant amplitude
$r$    Radius of the pin
$R$    Radius of the hole
$t$    Length of thickening area
$\Delta \theta$    Contact angle between pin and hole

## INTRODUCTION

It is known that mechanically fastened joining, such as pins, rivets, and bolts, is an important joining method widely applied to aerospace, construction, machinery, railway, and automotive industries because mechanical joining is the only form that permits disassembly without causing any damage to the structure.[1–6] Accurate and proper designs of mechanically fastened joints require the determination of stress distribution at the contact surface, which can determine the strength of joints.[7,8]

Three basic approaches are used to analyze the problems of failure mechanism, stress distribution, and stress concentration. The first and most mathematically rigorous approach is analytical method. Aluko et al.[9] Echavarría et al.,[10] and Wu et al.[11] have studied the stress distribution around a pin-loaded hole in elastic orthotropic composite plates by using the analytical method. The second approach uses numerical techniques, such as the

finite element method, to study the problems. Persson et al.,[12] have studied the delamination initiation of laminates with pin-loaded holes by using numerical techniques. The third approach is the experimental method, which can give a good demonstration by combining with the first two methods. Wang et al.[13] carried out an experimental investigation and design of extruded aluminum alloy T-stubs connected by swage-locking pins. Karakuzu et al.[14] studied the effect of hole positions on the failure behavior of glass-epoxy laminated composite plates fabricated from stacking sequences subjected to a traction force by three pins. Fiore et al.[15] investigated the bearing strength and failure behavior of pinned hybrid glass-flax composite laminates. Most of the studies focus on stress distribution and concentration under elastic deformation or failure mode for composite or nonferrous metals. In the case of using steel to make a pin connection structure, plastic deformation of the pin-loaded hole is unavoidable. Therefore, it is important to study the stress distribution and concentration of the pin-loaded hole under plastic deformation. However, there is little focus on stress distribution and concentration, deformation distribution, and changes of microstructures during plastic deformation, and experimental methods are rarely reported for studying these problems.

In general, it is widely accepted that there are three basic joint failure modes, which are net tension, shear out, and bearing.[5,16] However, in practice, the first two failure modes are catastrophic, and bearing is the most desired mode. Karakuzu et al.[16] have studied the effects of geometric parameters, such as the edge distance-to-hole diameter (E/D), the distance between two holes-to-hole diameter (M/D), and the distance from the upper or the lower edge of the specimen to the center of hole-to-hole diameter (K/D) ratio, on failure behavior in laminated composite plates with two parallel pin-loaded holes; they have studied the influence of different parameters on failure mode. They found that failure mode is shear out for E/D = 1, and the failure modes are the bearing of the specimens which have E/D > 1 and M/D > 2. Fiore et al.[5] have made an experimental failure map, clustering the main failure modes of pinned hybrid composite laminate, to better clarify the relationship between mechanical failure and geometrical parameters of joints. The results show that we can avoid catastrophic failures of structural joints and favor only a progressive failure mode by selecting specific geometrical parameters only in a narrow range of values.

Low carbon medium manganese steel can be widely used in vehicle, engineering machinery, building, structure[17–21], and many other important fields because of its high yield strength, high elongation, and low yield ratio.[22–31] One application example of this steel is the legs of an offshore platform, which is equipped with a lifting device

fixed by a pin, and the sketch diagrams of the offshore drilling platform and lifting device are shown in Fig. S1. A pin type lifting device is a common form of jack-up platform, which implements the lifting operation and supports the platform mainly relying on the coordination of the pin on a lifting device and holes on legs. Because the pin needs to be continuously plugged in and out of holes to implement lifting and lowering, there should be a certain clearance between the pin and hole. Due to the clearance between the pin and hole, their fit mode is totally different from that of the common shaft and sleeve, which are closely matched, and the clearance is very small. For the pin and hole, the contact area between the pin and hole is a very small area and will cause a serious stress concentration, so plastic deformation is inevitable. The stress concentration behavior of pin-loaded holes is often of great importance for the design of steel structures.

In this study, analytical and experimental methods were proposed to calculate the stress distribution around the pin-loaded hole with different clearances. The simulation of the symmetrical pin traction experiment of high strength and toughness medium manganese steel was carried out. The model of the tested specimen and pin is a reduced scale representation of the actual offshore platform. Stress distribution and concentration were calculated based on the experimental results and mechanical principle. The influences of the different clearances, thicknesses, and traction loads on stress distribution and concentration are studied. The changes of hardness distribution of different pin radiuses were investigated by hardness experiments. Microstructures before and after traction were observed through SEM experiments. The change of phase composition in the process of pin traction was studied by XRD experiments.

## EXPERIMENTAL METHODS

### Material

The composition of the studied material in this work is Fe-0.065C-0.2Si-5.45Mn (in wt.%). A continuous casting slab of 230 mm thickness was heated to 1150°C for 30 min, hot rolled to 30 mm and then water quenched to room temperature. The quenched steel was annealed at 630°C for 30 min to obtain a certain amount of RA. The yield and tensile strength of the tested steel are 690 MPa and 860 MPa, respectively, the yield ratio is 0.80, and the elongation rate is 35.8%.

### Simulation Symmetrical Pin Traction Experiment

To study the effects of clearance, thickness, and traction load on stress and plastic deformation distribution, 1:10 scale models of pin-loaded holes were conducted using a universal testing machine.
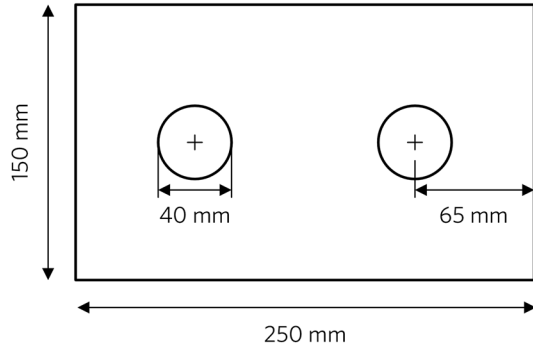
Fig. 1. Dimension of pin traction specimens.

Specimens are rectangular plates with 250 mm length and 150 mm width, and there are two symmetrical holes with 40 mm diameter in specimens, whose centers are 65 mm away from the short edge, as shown in Fig. 1. Specimens of three different thicknesses ($h$ = 5 mm, 8 mm, and 10 mm) were prepared to study the influence of thickness. Two different pin radiuses of 17 mm (Pin1) and 18.5 mm (Pin2) were chosen to study the influence of clearance. The specimens were set up on a universal testing machine (Zwick/Roell-Z1600) with special fixtures and pins, and the tensile rate is 0.1 mm/min at room temperature. The increase in diameter along the direction of the traction $\Delta D$ and maximum unilateral thickening of plate $\Delta h_0$ were measured by every 50 kN increase of the traction force. Stress distribution and concentration were calculated according to the parameters obtained from the experiments and mechanics principle.

## Microstructure Characterization and Hardness Experiment

The microstructure and hardness of 5-mm-thick specimens with different pin radiuses were analyzed when the traction force was 200 kN. Because the specimens are symmetrical along the straight line connected by centers of two holes, only half of the specimen was sampled, and the sampling position is shown in Fig. S2. Metallographic specimens with 6 mm length, 4 mm width, and 5 mm thickness were taken from the identical regions of the center of the original hole every 22.5° of 5-m- thick steel plates from 0° to 90°, and these specimens are also used to conduct hardness and XRD experiments. The faces of specimens facing the hole are used for microstructure observation and hardness experiments. Microstructure morphology observations were performed using a field emission scanning electron microscope (SEM, ZEISS ULTRA 55). The volume fraction of RA was measured by x-ray diffraction (XRD, SMART LAB 9 kW Cu K$_\alpha$). Vickers hardness was obtained by a micro-hardness meter.

## CALCULATION METHOD FOR DEFORMATION AND STRESS DISTRIBUTION

The influences of pin radius and specimen thickness on stress concentration under elastic condition have already been widely studied. However, it is inevitable that plastic deformation would take place in pin-loaded holes made by steels, and it is very important to study the deformation and stress distribution under plastic deformation. Medium manganese steel will not crack rapidly after deformation because of its low yield ratio and will uniformly thicken in the traction process, and it is assumed by macro-observation that plastic deformation will not affect the untouched area. In this experiment, to study the influences of clearance, thickness of specimens, and traction force on deformation and stress distribution, the increase in diameter along the direction of the traction $\Delta D$ and maximum unilateral thickening of plate $\Delta h_0$ were measured when the load increases by 50 kN.

The continuous part of the contact edge $\Delta \theta_i = \theta_2 - \theta_1 (i = 1, 2.)$, through which the loaded pin with a radius of $r_i (i = 1, 2.)$ traction forces into the plates, is regarded as a variational parameter (Fig. 2a and b). $\Delta \theta$ can be calculated by using the geometry analysis method (Eq. 1).

$$\Delta \theta = 2 arcsin \frac{R^2 - r^2 - (R - r + \Delta D)^2}{2r(R - r + \Delta D)} \quad (1)$$

For this problem, the unilateral thickening of the contact area is also approximated by a sinusoidal distribution on a continuous part of the contact edge. The unilateral thickening distribution along the edge can be written as Eq. 2 with the unilateral thickening amplitude $\Delta h_0$ (Fig. 2a, c, and d). The length of thickening $t$ can be calculated based on the constant volume principle in the process of the metal plastic deformation (Eq. 3)

$$\Delta h = \Delta h_0 \sin\left(\pi \frac{\varphi - \theta_1}{\theta_2 - \theta_1}\right) \quad (2)$$

$$t = \frac{h}{2\Delta h}\left[R + \Delta D - r + r\sin\varphi - \sqrt{R^2 - r^2 cos^2\varphi}\right] \quad (3)$$

In line with the previous approximation, the pin load is also approximated by a sinusoidal distribution of normal edge forces on a continuous part of the notch edge, as shown in the literature.[32,33] The boundary condition for the edge can be written as Eq. 4 with the force resultant amplitude, $p_0$, as shown in Fig. 2e.

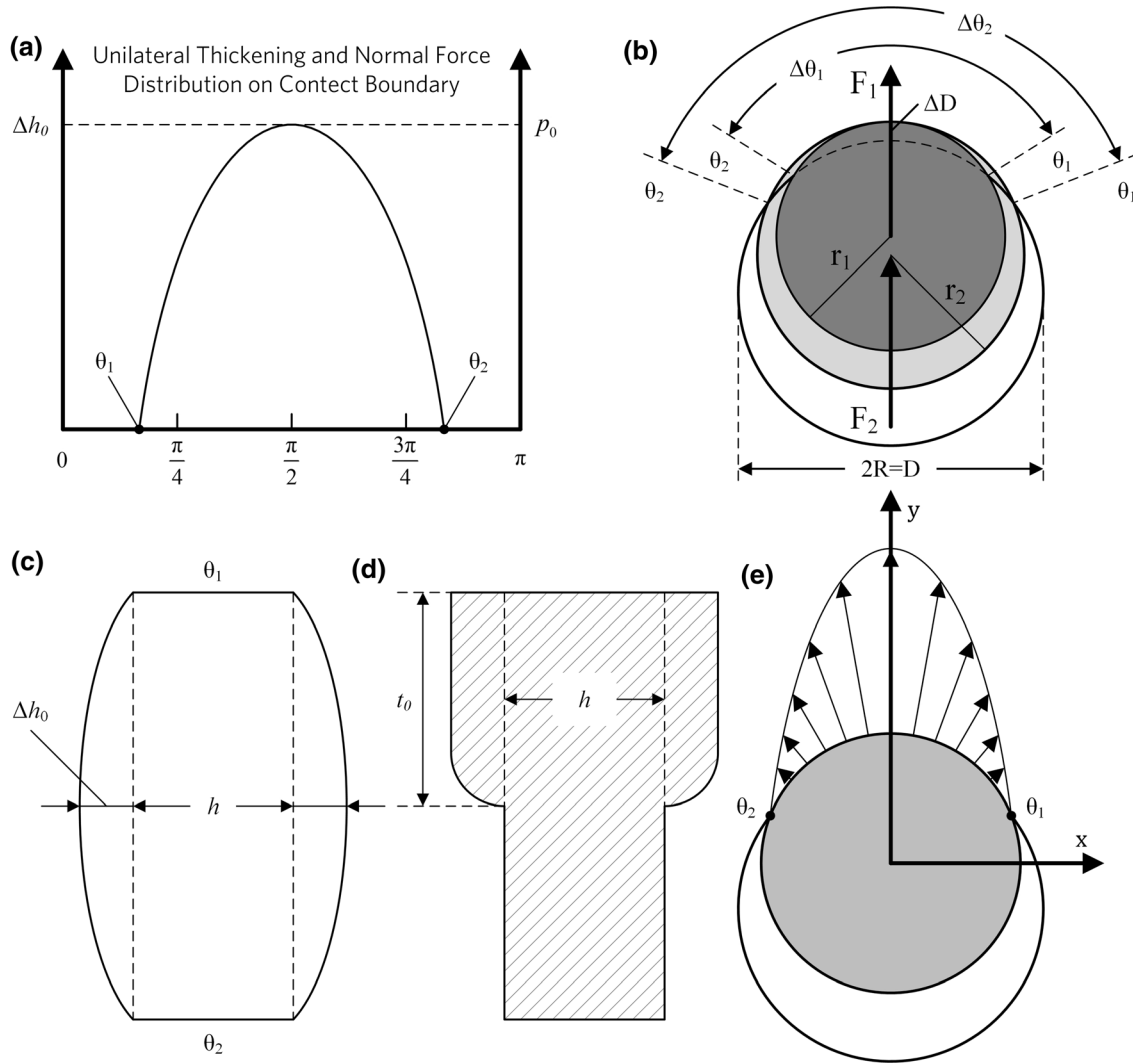$$p = p_0 \sin\left(\pi \frac{\varphi - \theta_1}{\theta_2 - \theta_1}\right) \quad (4)$$

Fig. 2. Model of normal force and deformation distribution at contact area (a), the influence of pin radius (b), schematic diagram of $\Delta h$ distribution (c), profile of $\Delta t_0$ (d), and schematic diagram of $p$ distribution (e).

Pin-load integral in the tensile force direction along contact edge can be determined by Eq. 5. Convert Eq. 5 into ordinary integrals and get (Eq. 6); the force resultant amplitude $p_0$ can be expressed by (Eq. 7).

$$F = \int_{\frac{\pi-\Delta\theta}{2}}^{\frac{\pi+\Delta\theta}{2}} sin\varphi p_0 sin\frac{\varphi-(\pi-\Delta\theta)/2}{\Delta\theta/\pi}\left[h + 2\Delta h sin\frac{\varphi-(\pi-\Delta\theta)/2}{\Delta\theta/\pi}\right]rd\varphi$$

(5)

$$\frac{F}{2rp_0} = h\int_{\frac{\pi-\Delta\theta}{2}}^{\frac{\pi}{2}} sin\varphi sin\frac{\varphi-(\pi-\Delta\theta)/2}{\Delta\theta/\pi}d\varphi + \Delta h\int_{\frac{\pi-\Delta\theta}{2}}^{\frac{\pi}{2}} sin\varphi d\varphi$$
$$- \Delta h\int_{\frac{\pi-\Delta\theta}{2}}^{\frac{\pi}{2}} sin\varphi cos\frac{2\varphi-(\pi-\Delta\theta)}{\Delta\theta/\pi}d\varphi \#$$

(6)

$$p_0 = \frac{F}{2r}\bigg/\left(\frac{h\pi\Delta\theta}{\pi^2-\Delta\theta^2}sin\frac{\pi-\Delta\theta}{2} + \frac{4\Delta h\pi^2}{4\pi^2-\Delta\theta^2}cos\frac{\pi-\Delta\theta}{2}\right)$$ (7)

## RESULTS

### Geometry Changes of Specimens During Pin Traction

Figure S3 shows macrographs of specimens with different thicknesses subjected to different traction loads and pin radiuses, where a, b, and c are 5 mm thick for 200 kN, 8 mm thick for 350 kN, and 10 mm thick for 450 kN of Pin1 and d, e, and f are 5 mm thick for 200 kN, 8 mm thick for 400 kN, and 10 mm thick for 500 kN of Pin2. As this figure shows, the 5-mm-thick outer contour is almost unchanged after a traction force of 200 kN for Pin1 and Pin2. However, the outer contour of 8- and 10-mm-thick specimens obviously changed, and outward bulges have been produced at the short edges of the specimens. This shows that the 8- and 10-mm-thick specimens have failed under these conditions. Another obvious phenomenon is that plastic deformation occurs

outwardly along the traction load direction at the contact area, and the radius of the deformation area is consistent with the pin. There is also some thickening in a certain range of the contact area. All the specimens with Pin1 have the same trend as those of Pin2, but the contact angle of Pin2 is larger than those of Pin1, so the pins with larger radiuses can withstand more traction.

Figure 3 shows the curves of increases in hole diameter along the direction and increases in unilateral thickening $\Delta h_0$ of the traction load $\Delta D$ of different $h$ and $r$ with $F$. $\Delta D$ exponentially increases with $F$, and $\Delta D$ of thicker specimens is smaller than that of the thinner specimen under the same $F$. Figure 3 also shows that $\Delta D$ of 5-mm-thick specimens is 1.8 mm for Pin1 and 1.5 mm for Pin2 under the $F$ of 200 kN. Combined with the macrograph results (Fig. S3a, d), the outer contour of the specimens is unchanged, which means deformation is not transferred to the edge of specimens in this dimension, clearance, and traction load condition; in other words, the specimen is not yet in failure. However, for the 8- and 10-mm-thick specimens, the increasing rate of $\Delta D$ suddenly gets faster once $F >$ 300 kN for 8-mm-thick specimens and 400 kN for 10-mm-thick specimens. Combined with the macrograph results (Fig. S3b, c, d, e), it was found that the

edges of specimens were seriously deformed. This shows that the deformation of the pin-loaded hole has been transferred to the edges of specimens. In this case, the specimen is already in failure mode, and this situation no longer applies to boundary conditions. Therefore, it can be considered that $\Delta D$ within 2 mm is safe, and only the deformation and stress analysis under safe state is considered. Figure 3c shows that $\Delta h_0$ s of Pin1 are all larger than those of Pin2 with the same $h$ and $F$. This is because larger $r$ can increase the contact area and thus reduce the stress concentration. $\Delta h_0$ also exponentially increases with $F$ and with the decrease of $h$ under the same $F$.

## Stress Distribution and Stress Concentration

Another important parameter is the contact angle of the specimen and pin $\Delta\theta$, which is calculated by substituting $\Delta D$ into Eq. 1. Figure 4 shows the curves of increases in $\Delta\theta$ of the specimens with different $h$ and $r$ with $F$. As Fig. 4 shows, $\Delta\theta$ increases almost linearly, and the increasing rates of $\Delta\theta$ of 5-mm-thick specimens are larger than those of 8 and 10 mm. However, the increasing rates of 8- and 10-mm-thick specimens are almost the same. Figure 4 also shows that the increasing rates of $\Delta\theta$ of Pin2 are all larger than those of Pin1.
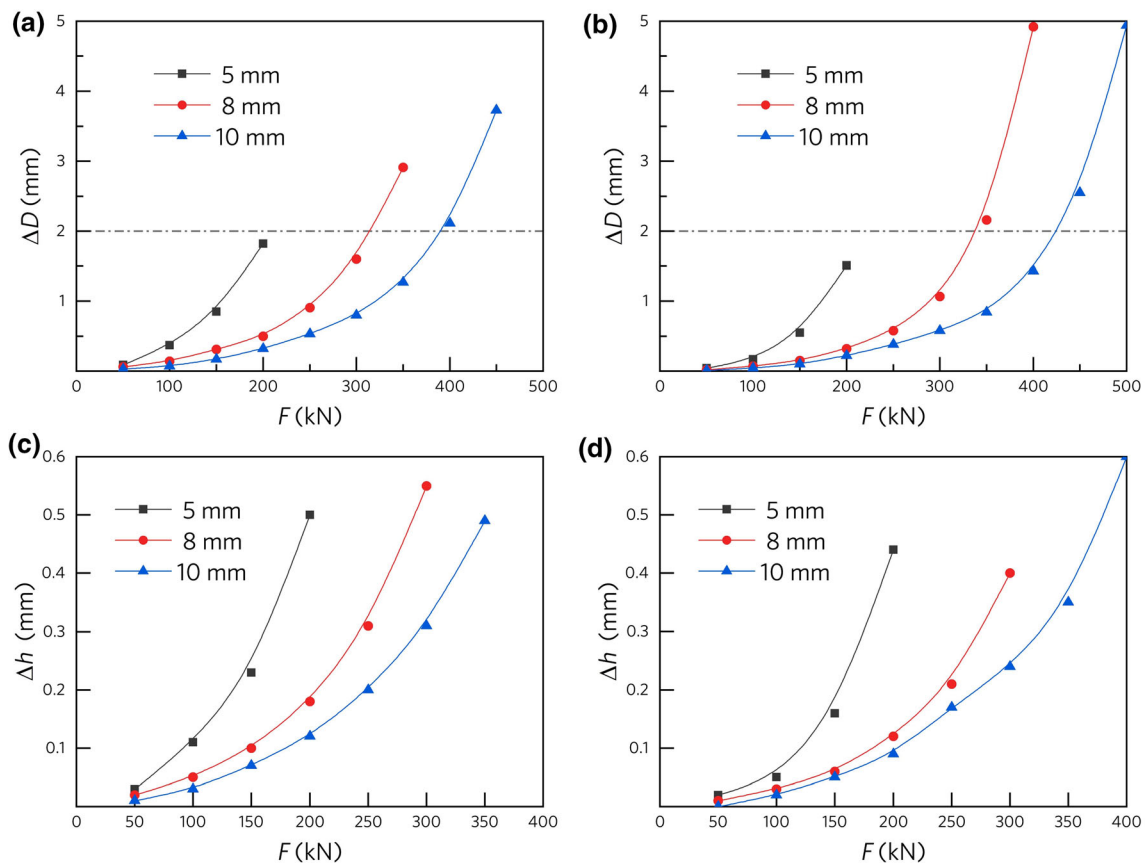


Fig. 3. Curves of increases in diameter along the direction of the traction of different specimen thicknesses under different traction loads. (a) Pin1 and (b) Pin2 and increase in unilateral thickening of plate of different specimen thicknesses under different traction loads. (c) Pin1; (d) Pin2.
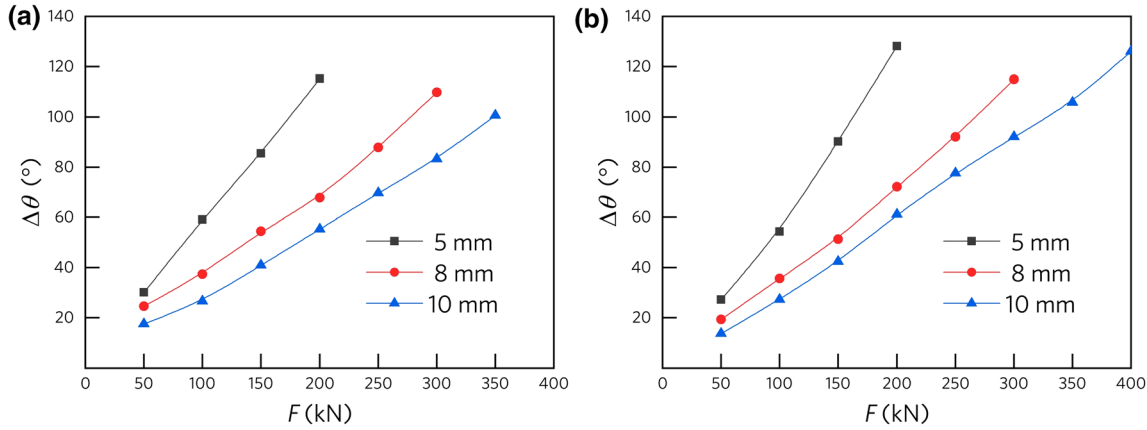
Fig. 4. Curves of increases in contact angle of different thicknesses under different traction loads. (a) Pin1; (b) Pin2.

Table SI shows the force resultant amplitude $p_0$ of different $h$ and $r$ under different $F$. $p_0$ was calculated by using the parameter measured from the specimens and Eq. 7. There is an obvious trend in Table SI that most of the maximum stresses of Pin1 are around 1950 MPa except for some small loads, such as the 5-mm-thick specimen with Pin1. $p_0$ increases with the load in small deformation and becomes steady when $F$ is 150 kN and 200 kN; this indicates that load has some influence on the stress concentration at the initial deformation. Nevertheless, the specimens with Pin2 have the same trend as those with Pin1, and the maximum stress is about 1700 MPa. The results indicate that the stress concentration is only related to the pin radius.

## Microstructure Characterization

Figure 5 shows the representative SEM microstructures for Pin1-1 (a), Pin1-19 (b), Pin2-1 (c), and Pin2-19 (d) of 5-mm-thick specimens, where position 1 only bears compressive stress and position 19 only bears tensile stress at the hole edge. Figure 5a and c shows that some thin martensite laths are presented among wide laths, and prior austenite grain boundaries become unobvious after pin traction, which is caused by compression deformation. It also can be seen that different $r$ has little effect on the volume fraction of fine laths. Position 1 has the largest stress and the highest deformation along the hole boundary under stress, and RA will transform into martensite during plastic deformation.

## Hardness Distribution

Figure 6 shows the hardness distribution measured around the pin-loaded hole of the 5-mm-thick specimen after deformation with a traction load of 200 kN. The results were treated as axisymmetric by 90° direction, where Fig. 6a is the result of the specimen with Pin1 and Fig. 6b is that with Pin2. As Fig. 6 shows, hardness increases obviously at the small region near the contact area, which is called

Region1, and the hardness of a large region in the direction of the traction load, which is called Region2, is also increased. In addition, as the same trend of $\Delta\theta$ variation with $r$, the contact angle of Region1 of the specimen with Pin2 is bigger than that of Pin1. Another obvious phenomenon is that the maximum hardness of the specimens with Pin1 (336 HV500) is higher than that of Pin2 (322 HV500), and the wideness of Region1 is about the same as the maximum length of thickening $t$. However, Region2 of the specimen with Pin1 is smaller than that of Pin2. Figure 6 shows that the radius of Region2 in 45° direction is larger than in the other direction. This means the length of the deformed region in this direction is the largest.

## XRD Result

Figure S4 shows the XRD spectrum of different positions of the 5-mm-thick specimen with Pin1 under 200 kN traction force, and the RA volume fractions of different positions are listed in Table SII according to Eqs. 8–9.[34,35]

$$V_{\alpha'} + V_{\gamma} = 1 \qquad (8)$$

$$V_{\gamma} = \frac{1.4 I_{\gamma}}{I_{\alpha'} + 1.4 I_{\gamma}} \qquad (9)$$

where $V_{\alpha'}$ is the volume fraction of martensite, $V_{\gamma}$ is the volume fraction of austenite, $I_{\alpha'}$ is the intensity of martensite, and $I_{\gamma}$ is the intensity of austenite.

The distribution diagram of the RA volume fraction was made according to the RA volume fraction listed in Table SII, and the results were treated as axisymmetric by 90° direction as shown in Fig. S5. As Table SII and Fig. S5 show, all the RA is transformed into martensite within a certain range of contact area, and the volume fraction of RA increases gradually with increasing radius. This result is in good agreement with the result of hardness distribution; in other word, the hardness increases with the transformation of RA to martensite. No RA remained within 8 mm along the 90°
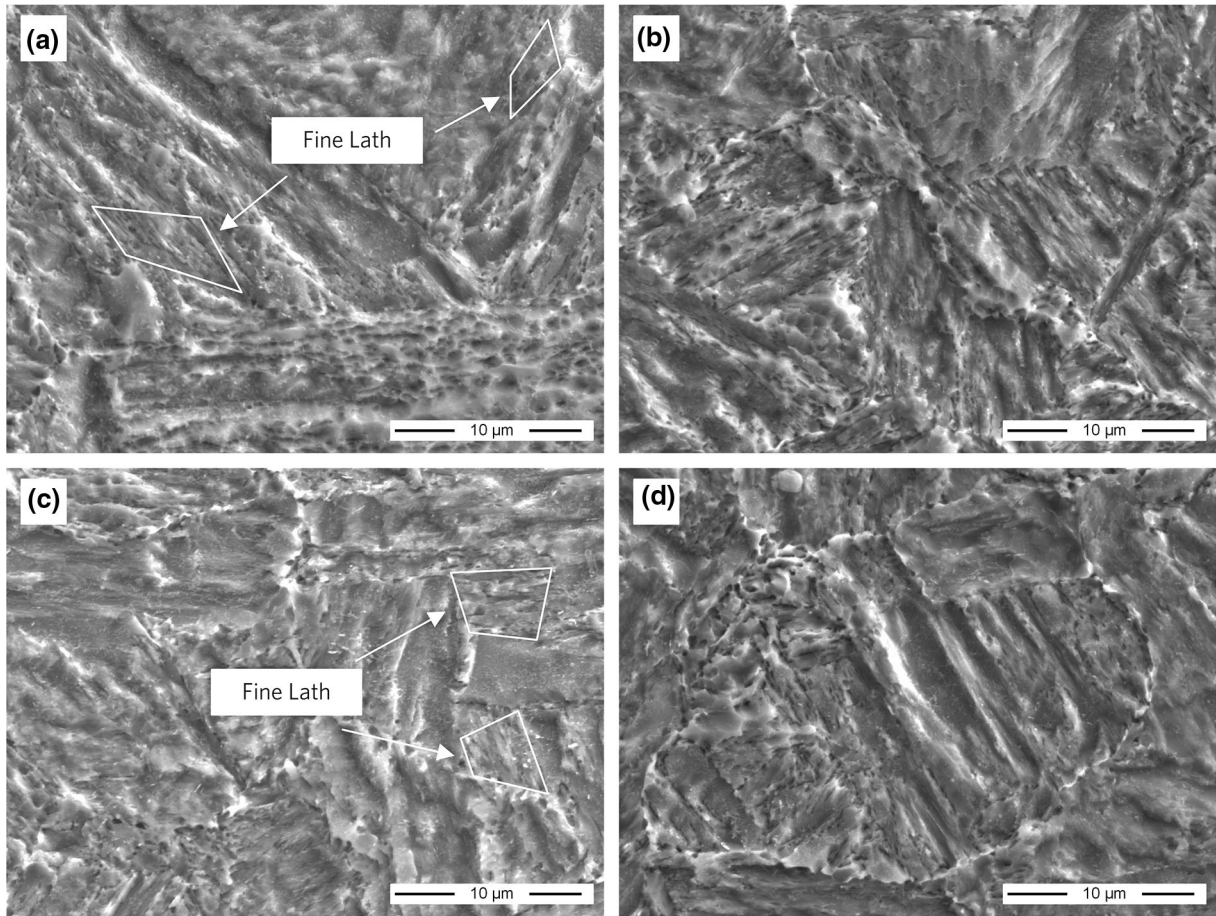
Fig. 5. SEM microstructures for Pin1-1 (a), Pin1-19 (b), Pin2-1 (c), and Pin2-19 (d) of 5-mm specimens under traction load of 200 kN.
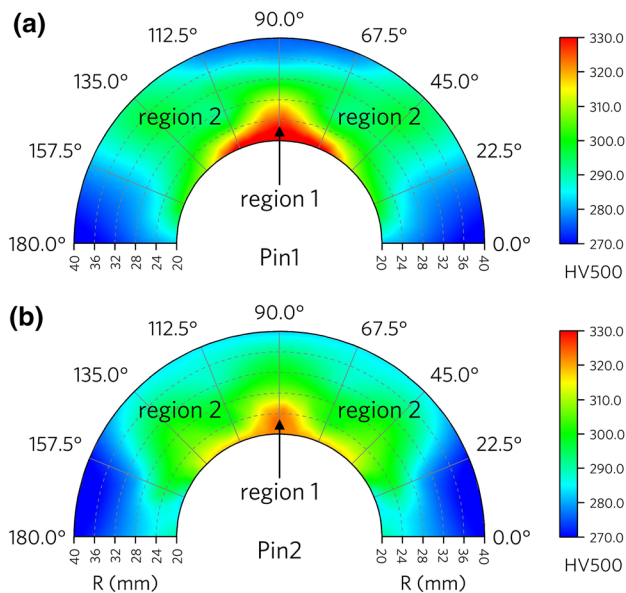


Fig. 6. Hardness distribution of 5-mm-thick specimen for Pin1 (a) and Pin2 (b).

direction or within 4 mm along the 67.5° direction, and some RA remained in the other direction along the hole boundary.

## DISCUSSION

### Effect of Specimen Dimensions and Clearance on Stress Distribution and Concentration

Stress concentration and distribution play an important role in the design of pin-loaded holes. Most researchers focus on the effect of specimen dimensions on failure mode or stress concentration calculation by analytical method and assume that only elastic deformation arises in pin joints, which act as the main connection method in the composite and some non-ferrous metals. However, pin-loaded holes in lifting devices of offshore platforms will generate slight plastic deformation at contact regions, which is caused by using a clearance fit. The steel used in this study has good toughness, so only one failure mode can occur, that is, bearing mode. In this circumstance, the contact angle and stress concentration are two important parameters reflecting stress distribution, which are affected by geometric dimensions of pin and hole. Therefore, the traction load, plate thickness, and pin radius are the

main factors affecting stress concentration and distribution.

To better understand the relationship between $F$ and stress concentration, the calculation results of stress of the 5-mm-thick specimen with Pin1 under different $F$ were used to draw the curves of stress distribution, as shown in Fig. 7a. It is obvious that $p_0$ increases with $F$ at the initial traction, but increases just a little from 150 kN to 200 kN. According to the general knowledge of geometry, it can be considered that the contact area between holes and pins with different radiuses is a line when there is no traction load. Once the traction starts, theoretically the stress on this line will be infinite and the steel will deform and yield, so plastic deformation is inevitable. Furthermore, $\Delta\theta$ increases during deformation and the stress concentration decreases rapidly. Hence, the deformation stops because of the combined action of work hardening and geometric constraints. Work-hardening degree is small at the initial traction due to the small plastic deformation; therefore, the peak stress increases obviously with the increase of $F$. As the traction goes on, the deformation degree of the deformed area further increases, which is also shown in the increase of $\Delta h_0$, $\Delta D$, and $\Delta\theta$, and the work-hardening degree also increases. The deformation not only transferred to the surrounding area, but also thickened the deformed area. Therefore, $p_0$ will not continue to increase when the deformed area has hardened enough to resist pin traction. $p_0$ increases just a little when $F > 150$ kN and reaches 200 kN; this means greater loads mainly lead to the increase of deformation area by increasing $\Delta\theta$ instead of $p_0$. $p_0$ of the specimens with Pin1 is steady at about 1950 MPa, and similar results were obtained for other specimens also with Pin1.

Meanwhile, the thickness of steel and clearance also deeply influence the stress concentration and distribution. Figure 7b, c and d shows the stress distribution curves of different $h$ and $r$ under the same $F$ of 200 kN. Figure 7b shows that $p_0$ of Pin1 is larger and $\Delta\theta$ of Pin1 is smaller than Pin2. This means the larger the pin radius is, the greater the $\Delta\theta$ and the smaller the $p_0$. The above rule is also obeyed for all the specimens with different thicknesses, as shown in Fig. 7c and d. In addition, another obvious phenomenon in Fig. 7 is that $\Delta\theta$ decreases with $h$ under the same $F$ and $r$. Combined with the results of $\Delta\theta$ variation with $F$, thicker specimens can bear more traction load when reaching the same $\Delta\theta$. Specimen thickness can reflect the structure stability, which will be broken once the load reaches a critical value of the specimen under compressive stress. Furthermore, the deformation increases dramatically when the traction load is beyond the critical value, which should be avoided during service. It can also be seen that in the later period of traction, $p_0$ does not change with the $F$ and $h$ when traction exceeds a certain value. $p_0$ of the specimens with Pin1 and Pin2 are maintain steady at about 1950 MPa and 1700 MPa, respectively. Overall, clearance is the main factor influencing stress concentration.

It is widely accepted in the literature that there are three fit methods to join the pin and hole, which are interference fit, transition fit, and clearance fit. Interference fit is thought to be able to improve the mechanical performance of joints by introducing residual compressive stress and has drawn the attention of researchers in the past years. In interference fit, the contact angle will be 360°
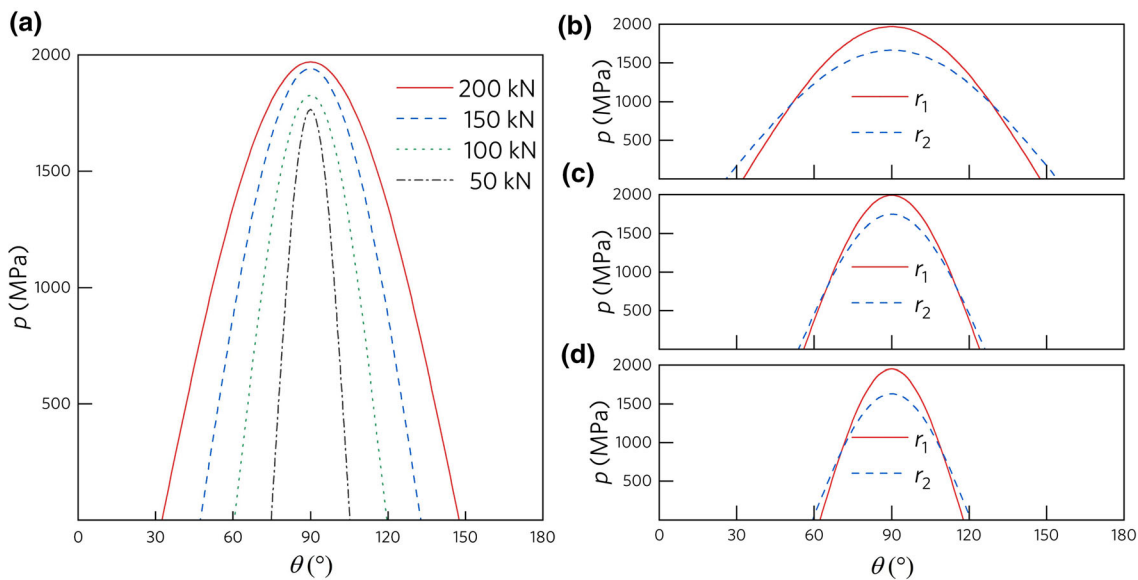


Fig. 7. Stress distribution of 5-mm specimen with 17-mm pin radius under different loads (a) and stress distribution of different thicknesses under 200 kN load. (b) 5 mm, (c) 8 mm, (d) 10 mm.

unless the traction load is greater than the resultant force of residual compressive stress for 180°. In transition fit, the contact angle will become 180° once the load starts and does not increase or decrease. However, in clearance fit, the size of clearance is an important parameter affecting stress distribution and deformation distribution. To ensure the smooth operation of the transmission facilities of the lifting device, the balance must be found in the design of the pin-loaded hole among stress concentration, plate thickness, and clearance. Our results show that the stress concentration decreases with clearance when the lifting device operates smoothly.

## Plastic Deformation of Pin-Loaded Hole During Traction

In this study, the plastic deformation is mainly reflected in the increase of $R$ and $h$. However, to ensure the structural safety, $\Delta D$ must be in a certain range. It is recognized that plastic deformation of the hole in clearance fit is inevitable. At the same time, plastic deformation is also the main reason for bearing large loads without failure. For medium manganese steel, the increase of hardness during plastic deformation is accompanied by RA SIMT and deformation hardening of the martensite matrix. Therefore, the hardness change of the specimen reflects the degree of plastic deformation.

The graph of hardness distribution (Fig. 6) shows that the hardness of Region1 with Pin1 is much larger than that with Pin2, and the hardnesses of Region2 with Pin1 and Pin2 are similar. The main reason for this phenomenon should be the different hardening mechanisms, which are SIMT and work-hardening effect. At the beginning of deformation, RA will deform first because of its low strength and high plasticity; therefore, the hardness increase of Region2 was caused by SIMT of RA. With ongoing traction, most of the deformation is concentrated in Region1, so, the reasons for hardening of Region1 are both SIMT and work-hardening effect. Figure 6 shows that the sizes of the areas where the hardnesses increase are different, where the area with Pin1 is smaller than that with Pin2. This indicates that the larger the clearance is, the greater the maximum deformation and the smaller hardening area under the same $F$. The angle of hardness increase can also be seen in Fig. 6, showing that the hardening distance in the direction of 45° is the largest. This result has good consistency with many conclusions in the literature, i.e., the maximum shear stress appears in 45° direction.

On the other hand, the degree of deformation is also affected by specimen thickness and traction load, which can be determined by the unilateral thickening amplitude $\Delta h_0$ and the maximum length of thickening $t_0$. Figure 8 shows the $t_0$ of different $h$ and $r$ under $F$ of 200 kN. $t_0$ increases with $h$ because thicker specimens have better structural stability.
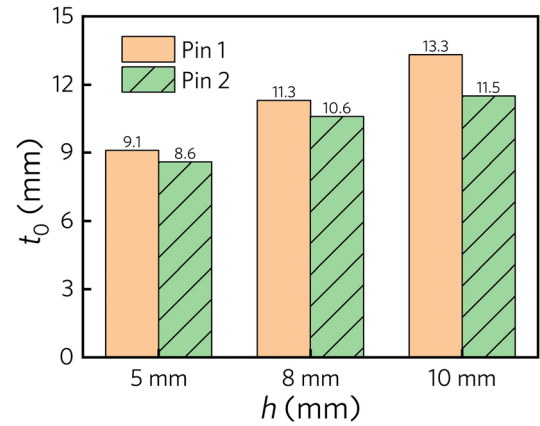


Fig. 8. Maximum length of thickening $t_0$ of different specimen thicknesses and pin radius under 200 kN traction load.

This will make the deformation extend to further regions. However, $t_0$ of Pin1 is larger than that of Pin2 for the specimens of all thicknesses; this is because the larger the clearance is, the smaller the $r$, which will result in greater stress concentration and thus increase the degree of deformation.

Here, the plastic deformation process can be described as follows. Before the traction starts, the contact area between the hole and the pin with different radiuses is a line. When the traction starts, the local deformation is started once the specimen exceeds the stress limit with the increase of load since the contact line expands to both sides of the edge of the hole. During this period, SIMT occurs and dislocation increases in the martensite matrix around contact area. As the traction continues, the pin invades into the specimens and the deformation area is divided into two parts; one region is thickened (Region1) and the other region is unthickened (Region2). The deformed structure can bear more traction load because of the work-hardening effect and SIMT, and the contact area becomes larger because the stress concentration cannot make the initial deformation area continue to deform; deformation can only be transferred far away and will lead to the contact angle and unilateral thickening increase.

## Microstructure Changes of Specimens During Pin Traction

Low carbon medium manganese steel can be widely used in many fields because of its high strength, excellent toughness, and cost-effectiveness. The improved combination of strength and toughness was obtained via intercritical annealing, and metastable austenite was stabilized at room temperature via enrichment of Mn during annealing process. The change of microstructure is accompanied by the deformation of the pin-loaded hole of medium manganese steel during traction, which has two typical characteristics: one is that dislocation increases by the deformation of martensite

matrix; the other is RA in steel transforms into martensite induced by strain. These two characteristics work together to produce deformation strengthening.

Combined with XRD results, in a certain range of contact area, the volume fraction of RA is 0, which means that RA is all transformed into martensite, and the size of this area corresponds to the area with the highest hardness. Similarly, the volume fraction of RA and hardness changes with the degree of deformation according to the results of other regions. The degree of deformation can directly reflect the change of microstructure. The SEM photograph shows some obvious difference between the large and small deformation area. Some fine martensite laths appear in the large deformation area but do not appear in the small deformation area; these are produced through SIMT. The XRD results show that the furthest deformation propagation direction is in about the 45° rather than 90° direction. The reason for this phenomenon is that the maximum shear stress appears at 45° direction.

Furthermore, the stability of RA, which is very important for strength and toughness, plays an important role in the safety of the pin-loaded hole for medium manganese steel. For the structure of the hole, the stability of RA has a great influence on plastic deformation and its transferring. If the stability of RA is too high, deformation cannot be transferred because the specimen near the contact area will always deform until SIMT has been completed. However, if the stability of RA is too low, SIMT occurs at the early phase of plastic deformation, which will reduce toughness. Both of these situations will reduce the safety and increase the risk of failure. Therefore, the stability of RA should be controlled in a reasonable range, which is mainly controlled by the content of C and Mn in RA phase.

## CONCLUSION

Pin hole with clearance is an important joint method in practical application. It is necessary to understand the distribution of stress and deformation during the structural design of the pin-loaded hole, especially in the presented case of local plastic deformation. In this study, we designed an experiment called the simulation symmetrical pin traction experiment, and it was the first time that this method was used in this kind of research. The actual service condition of the lifting device was studied by a simulation symmetrical pin traction experiment. The effect of geometry on stress distribution and concentration was calculated by analytical methods. Plastic deformation distribution and microstructure change were studied through hardness and XRD experiments. We reached the following conclusions:

1. At the beginning of the traction, both the contact angle between the pin and hole $\Delta\theta$ and force resultant amplitude $p_0$ increase with the traction load. As the traction continues, $p_0$ will be steady and only $\Delta\theta$ increases with the traction load.
2. The stress concentration increases with the decrease of radius of the pin $r$ and does not change with other parameters under the same $r$. Local deformation degree also increases with the decrease of $r$.
3. The increase of specimen thickness can only reduce $\Delta\theta$ but not the stress concentration, and thicker specimens can bear more traction load when reaching the same $\Delta\theta$.
4. Strengthening during deformation is caused not only by the increase of dislocation in martensite matrix but also by retained austenite strain-induced martensite transformation, which is conducive to the transfer of plastic deformation.

## CONFLICT OF INTEREST

We declare that we have no financial and personal relationships with other people or organizations that can inappropriately influence our work.

## SUPPLEMENTARY INFORMATION

The online version contains supplementary material available at https://doi.org/10.1007/s11837-021-04881-x.

## REFERENCES

1. F. Gamdani, R. Boukhili, and A. Vadean, *Mater. Des.* 88, 702. (2015).
2. H. Bazvandi and E. Poursaeidi, *Eng. Fail. Anal.* 111, 104443 (2020).
3. Y. Xu, H. Zhu, W. Xu, and C. Liu, *Int. J. Heat. Mass. Transf.* 125, 629. (2018).
4. R. Karakuzu, N. Taylak, B.M. İçten, and M. Aktaş, *Compos. Struct.* 85, 1. (2008).
5. V. Fiore, L. Calabrese, T. Scalici, and A. Valenza, *Compos. B. Eng.* 187, 107864 (2020).
6. Z. Zhang, W. Wang, C. Rans, and R. Benedictus, *Procedia Struct. Integr.* 2, 3361. (2016).
7. B. Grüber, W. Hufenbach, L. Kroll, M. Lepper, and B. Zhou, *Compos. Sci. Technol.* 67, 1439. (2007).
8. T.S. Kim, and H. Kuwamura, *Mater. Des.* 32, 3942. (2011).
9. O. Aluko, and H.A. Whitworth, *Compos. Struct.* 86, 308. (2008).
10. C. Echavarría, P. Haller, and A. Salenikovich, *Compos. Struct.* 79, 107. (2007).
11. T. Wu, K. Zhang, H. Cheng, P. Liu, D. Song, and Y. Li, *Compos. B. Eng.* 100, 176. (2016).

12. E. Persson, E. Madenci, and I. Eriksson, *Theor. Appl. Fract. Mech.* 30, 87. (1998).
13. Z. Wang, Y. Wang, Y. Zhang, L. Gardner, and Y. Ouyang, *Eng. Struct.* 200, 109675 (2019).
14. R. Karakuzu, C.R. Çalışkan, M. Aktaş, and B.M. İçten, *Compos. Struct.* 82, 225. (2008).
15. V. Fiore, L. Calabrese, T. Scalici, P. Bruzzaniti, and A. Valenza, *Polym. Test.* 69, 310. (2018).
16. R. Karakuzu, O. Demirgoren, B.M. Icten, and M.E. Deniz, *Mater. Des.* 31, 3029. (2010).
17. Z.Z. Zhao, R.H. Cao, J.H. Liang, F. Li, C. Li, and S.F. Yang, *JOM-US* 70, 700. (2018).
18. G.Q. Su, X.H. Gao, D.Z. Zhang, L.X. Du, J. Hu, and Z.G. Liu, *JOM-US* 70, 672. (2018).
19. R. Alturk, L.G. Hector Jr., M. Enloe, F. Abu-Farha, and T.W. Brown, *JOM-US* 70, 894. (2018).
20. R. Rana, E. De Moor, J.G. Speer, and D.K. Matlock, *JOM-US* 70, 706. (2018).
21. S. Pani, S.K. Singh, and B.K. Mohapatra, *JOM-US* 68, 1525. (2016).
22. J. Zhao, and Z. Jiang, *Prog. Mater. Sci.* 94, 174. (2018).
23. Y.K. Lee, and J. Han, *Mater. Sci. Technol.* 31, 843. (2015).
24. J. Hu, L.X. Du, W. Xu, J.H. Zhai, Y. Dong, Y.J. Liu, and R.D.K. Misra, *Mater. Charact.* 136, 20. (2017).
25. H. Liu, L.X. Du, J. Hu, H.Y. Wu, and R.D.K. Misra, *J. Alloys Compd.* 695, 2072. (2017).
26. X.Y. Qi, L.X. Du, J. Hu, and R.D.K. Misra, *Mater. Sci. Eng. A* 718, 471. (2018).
27. H. Luo, J. Shi, C. Wang, W. Cao, X. Sun, and H. Dong, *Acta Mater.* 59, 4002. (2011).
28. B.B. He, B.M. Huang, S.H. He, Y. Qi, H.W. Yen, and M.X. Huang, *Mater. Sci. Eng. A* 724, 11. (2018).
29. H. Lee, M.C. Jo, S.S. Sohn, A. Zargaran, and S. Lee, *Acta Mater.* 147, 247. (2018).
30. J. Hu, L. Du, G. Sun, H. Xie, and R.D.K. Misra, *Scr. Mater.* 104, 87. (2015).
31. Y. Du, X. Gao, L. Lan, X. Qi, H. Wu, L. Du, and R.D.K. Misra, *Int. J. Hydrog. Energ.* 44, 32292. (2019).
32. P.D. Mangalgiri, T.S. Ramamurthy, B. Dattaguru, and A.K. Rao, *Int. J. Mech. Sci.* 29, 577. (1987).
33. F. Chang, R.A. Scott, and G.S. Springer, *J. Compos. Mater.* 16, 470. (1982).
34. Y.H. Fan, B. Zhang, H.L. Yi, G.S. Hao, Y.Y. Sun, J.Q. Wang, E.H. Han, and W. Ke, *Acta Mater.* 139, 188. (2017).
35. B. Zhang, L.X. Du, Y. Dong, D.X. Han, H.Y. Wu, F.H. Lu, and R.D.K. Misra, *Mater. Sci. Eng. A* 771, 138643 (2020).